Research Article | Vol. 25, No. 13 | 26 Jun 2017 | OPTICS EXPRESS 14148
Optics EXPRESS

Chiral near-field manipulation in Au-GaAs hybrid hexagonal nanowires

EMILIJA PETRONIJEVIC,[1,*] MARCO CENTINI,[1] ALESSANDRO BELARDINI,[1] GRIGORE LEAHU,[1] TEEMU HAKKARAINEN,[2] AND CONCITA SIBILIA[1]

[1]*Department S.B.A.I., Sapienza Università di Roma, Department S.B.A.I., Via A. Scarpa 14, I-00161 Rome, Italy*
[2]*Optoelectronics Research Centre, Tampere University of Technology, Korkeakoulunkatu 3, 33720 Tampere, Finland*
**emilija.petronijevic@uniroma1.it*

Abstract: We demonstrate the control of enhanced chiral field distribution at the surface of hybrid metallo-dielectric nanostructures composed of self-assembled vertical hexagonal GaAs-based nanowires having three of the six sidewalls covered with Au. We show that weakly-guided modes of vertical GaAs nanowires can generate regions of high optical chirality that are further enhanced by the break of the symmetry introduced by the gold layer. Changing the angle of incidence of a linearly polarized plane wave it is possible to tailor and optimize the maps of the optical chirality in proximity of the gold plated walls. The low cost feasibility of the sample combined to the simple control by using linearly polarized light and the easy positioning of chiral molecules by functionalization of the gold plates make our proposed scheme very promising for enhanced enantioselective spectroscopy applications.

OCIS codes: (160.0160) Materials; (160.1585) Chiral media.

References and links

1. Z. Wang, F. Cheng, T. Winsor, and Y. Liu, "Optical chiral metamaterials: a review of the fundamentals, fabrication methods and applications," Nanotechnology **27**(41), 412001 (2016).
2. H. K. Bisoyi and Q. Li, "Light-directing chiral liquid crystal nanostructures: from 1D to 3D," Acc. Chem. Res. **47**(10), 3184–3195 (2014).
3. C. Wu, N. Arju, G. Kelp, J. A. Fan, J. Dominguez, E. Gonzales, E. Tutuc, I. Brener, and G. Shvets, "Spectrally selective chiral silicon metasurfaces based on infrared Fano resonances," Nat. Commun. **5**, 3892 (2014).
4. V. K. Valev, J. J. Baumberg, B. De Clercq, N. Braz, X. Zheng, E. J. Osley, S. Vandendriessche, M. Hojeij, C. Blejean, J. Mertens, C. G. Biris, V. Volskiy, M. Ameloot, Y. Ekinci, G. A. Vandenbosch, P. A. Warburton, V. V. Moshchalkov, N. C. Panoiu, and T. Verbiest, "Nonlinear superchiral meta-surfaces: tuning chirality and disentangling non-reciprocity at the nanoscale," Adv. Mater. **26**(24), 4074–4081 (2014).
5. V. K. Valev, J. J. Baumberg, C. Sibilia, and T. Verbiest, "Chirality and chiroptical effects in plasmonic nanostructures: fundamentals, recent progress, and outlook," Adv. Mater. **25**(18), 2517–2534 (2013).
6. D. H. Kwon, P. L. Werner, and D. H. Werner, "Optical planar chiral metamaterial designs for strong circular dichroism and polarization rotation," Opt. Express **16**(16), 11802–11807 (2008).
7. J. K. Gansel, M. Thiel, M. S. Rill, M. Decker, K. Bade, V. Saile, G. von Freymann, S. Linden, and M. Wegener, "Gold helix photonic metamaterial as broadband circular polarizer," Science **325**(5947), 1513–1515 (2009).
8. E. Hendry, T. Carpy, J. Johnston, M. Popland, R. V. Mikhaylovskiy, A. J. Lapthorn, S. M. Kelly, L. D. Barron, N. Gadegaard, and M. Kadodwala, "Ultrasensitive detection and characterization of biomolecules using superchiral fields," Nat. Nanotechnol. **5**(11), 783–787 (2010).
9. Y. Tang and A. E. Cohen, "Enhanced enantioselectivity in excitation of chiral molecules by superchiral light," Science **332**(6027), 333–336 (2011).
10. T. Kan, A. Isozaki, N. Kanda, N. Nemoto, K. Konishi, H. Takahashi, M. Kuwata-Gonokami, K. Matsumoto, and I. Shimoyama, "Enantiomeric switching of chiral metamaterial for terahertz polarization modulation employing vertically deformable MEMS spirals," Nat. Commun. **6**, 8422 (2015).
11. G. Leahu, E. Petronijevic, A. Belardini, M. Centini, C. Sibilia, T. Hakkarainen, E. Koivusalo, M. Rizzo Piton, S. Suomalainen, and M. Guina, "Evidence of optical circular dichroism in GaAs-based nanowires partially covered with gold," Adv. Opt. Mater. **2017**, 1601063 (2017).
12. M. Bertolotti, A. Belardini, A. Benedetti, and C. Sibilia, "Second harmonic circular dichroism by self-assembled metasurfaces," J. Opt. Soc. Am. B **32**(7), 1287–1293 (2015).

#290353 https://doi.org/10.1364/OE.25.014148
Journal © 2017 Received 10 Mar 2017; revised 19 Apr 2017; accepted 24 Apr 2017; published 13 Jun 2017

Optics EXPRESS

13. A. Belardini, M. C. Larciprete, M. Centini, E. Fazio, C. Sibilia, D. Chiappe, C. Martella, A. Toma, M. Giordano, and F. Buatier de Mongeot, "Circular dichroism in the optical second-harmonic emission of curved gold metal nanowires," Phys. Rev. Lett. **107**(25), 257401 (2011).
14. A. Belardini, M. Centini, G. Leahu, E. Fazio, C. Sibilia, J. W. Haus, and A. Sarangan, "Second harmonic generation on self-assembled tilted gold nanowires," Faraday Discuss. **178**, 357–362 (2015).
15. A. Belardini, M. Centini, G. Leahu, D. C. Hooper, R. Li Voti, E. Fazio, J. W. Haus, A. Sarangan, V. K. Valev, and C. Sibilia, "Chiral light intrinsically couples to extrinsic/pseudo-chiral metasurfaces made of tilted gold nanowires," Sci. Rep. **6**(1), 31796 (2016).
16. D. C. Hooper, A. G. Mark, C. Kuppe, J. T. Collins, P. Fischer, and V. K. Valev, "Strong rotational anisotropies affect nonlinear chiral metamaterials," Adv. Mater. **29**(13), 1605110 (2017).
17. Y. Tang and A. E. Cohen, "Optical chirality and its interaction with matter," Phys. Rev. Lett. **104**(16), 163901 (2010).
18. M. Schäferling, X. Yin, and H. Giessen, "Formation of chiral fields in a symmetric environment," Opt. Express **20**(24), 26326–26336 (2012).
19. T. J. Davis and E. Hendry, "Superchiral electromagnetic fields created by surface plasmons in nonchiral metallic nanostructures," Phys. Rev. B **87**(8), 085405 (2013).
20. M. Schäferling, D. Dregely, M. Hentschel, and H. Giessen, "Tailoring enhanced optical chirality: design principles for chiral plasmonic nanostructures," Phys. Rev. X **2**(3), 031010 (2012).
21. M. Finazzi, P. Biagioni, M. Celebrano, and L. Duò, "Quasistatic limit for plasmon-enhanced optical chirality," Phys. Rev. B **91**(19), 195427 (2015).
22. T. V. Hakkarainen, A. Schramm, J. Mäkelä, P. Laukkanen, and M. Guina, "Lithography-free oxide patterns as templates for self-catalyzed growth of highly uniform GaAs nanowires on Si(111)," Nanotechnology **26**(27), 275301 (2015).
23. G. Leahu, E. Petronijevic, A. Belardini, M. Centini, R. Li Voti, T. Hakkarainen, E. Koivusalo, S. Suomalainen, M. Guinda, and C. Sibilia, "Photo-acoustic spectroscopy revealing resonant absorption of self-assembled GaAs-based nanowires," Sci. Rep. (to be published).
24. M. H. Alizadeh and B. M. Reinhard, "Emergence of transverse spin in optical modes of semiconductor nanowires," Opt. Express **24**(8), 8471–8479 (2016).
25. K. T. Fountaine, W. S. Whitney, and H. A. Atwater, "Resonant absorption in semiconductor nanowires and nanowire arrays: Relating leaky waveguide modes to Bloch photonic crystal modes," J. Appl. Phys. **116**(15), 153106 (2014).
26. Lumerical Solutions, Inc., http://www.lumerical.com/tcad-products/fdtd/
27. D. R. Abujetas, R. Paniagua-Domínguez, and J. A. Sánchez-Gil, "Unraveling the janus role of mie resonances and leaky/guided modes in semiconductor nanowire absorption for enhanced light harvesting," ACS Photonics **2**(7), 921–929 (2015).
28. A. Henneghien, B. Gayral, Y. Désières, and J. Gérard, "Simulation of waveguiding and emitting properties of semiconductor nanowires with hexagonal or circular sections," J. Opt. Soc. Am. B **26**(12), 2396–2403 (2009).

1. Introduction

Chirality, the absence of mirror symmetry present in many important molecules and DNA, has fascinated the nanoscale community for many years now: nanostructures that possess geometric chirality (broken symmetry), interact differently with circularly polarized light of opposite handedness [1]. This engineered chiral response has been found in 1D [2], 2D [3–6] and 3D [7] nanostructures, and many applications in detection and characterization of biomolecules [8], enantioselectivity [9], polarization-sensitive devices [10] have been proposed. The collective effects in these nanostructures can be characterized by means of e.g. photo-acoustic technique or second harmonic generation [11–16]; however, applications based on the enhanced interaction between nanostructures and chiral molecules require more profound investigation and understanding of near field chiral effects. In fact it has been shown that the local value of the optical chirality governs the processes of circular dichroism: different absorption for differently headed fields in a medium [17].

For any monochromatic electromagnetic wave defined by electric (magnetic) field $\vec{E}$ ($\vec{B}$) complex amplitudes and frequency ω, the optical chirality can be expressed as [17,18]:

$$C = -\frac{\varepsilon_0 \omega}{2} \mathrm{Im}\left[\vec{E}^*(\vec{r}) \cdot \vec{B}(\vec{r})\right]. \quad (1)$$

For a plane wave propagating in free space, the absolute value of C is at maximum for circularly polarized wave (CPW), and zero for linearly polarized wave. This is due to the

Optics EXPRESS

condition imposed by Eq. (1): $\vec{E}$ and $\vec{B}$ need to have parallel components that are out of phase.

Beside the case of circularly polarized wave, nonzero values of C can be achieved in the near field of the medium that support evanescent waves. The term "superchiral" has been used to define a field with local values of C higher than the CPW limit. For example in [8] it has been shown enhanced enantioselectivity due to localized surface plasmon polariton excitations in plasmonic chiral nanostructures, responsible of "superchiral" fields. In [18] it was underlined that high local values of optical chirality are not necessarily related to a lack of symmetry in the nanostructure itself (geometrical chirality). It was then shown that even symmetric nanostructures such as plasmonic rod nanoantennas can exhibit optical chirality enhancement when excited by a linearly polarized wave [19]. In [20] different schemes are proposed with the aim to combine local field enhancements due to plasmon resonance and near field patterns with high values of local optical chirality.

However, looking at typical near field distributions it has been noticed that regions of a particular sign of the optical chirality are alternated to regions with opposite sign. Thus, for enhanced enantioselective spectroscopy it is necessary that chiral molecules need to be positioned only in regions with the same sign of optical chirality C. Indeed, the effect of the enhancement due to a group of molecules can be canceled or weakened by averaging the contributions coming from regions where the optical chirality has opposite sign values. Localization of molecules in specific regions where the nanostructure generates concentrated local fields of high optical chirality is of crucial importance in order to see a net enhancement on selectivity as also shown in [21].

In this work, we propose a geometry where optical chirality and positioning of the molecules could be easily controlled and achieved by taking advantage of properties of hybrid metallo-dielectric structures. The structure under examination is composed of vertical GaAs-based NWs of hexagonal cross section, hybridized with Au. The symmetry of the semiconductor NWs is broken by the presence of a non-uniformly deposited layer of gold partially covering the sidewalls. The fabrication of such NWs by molecular beam epitaxy on p-Si(111) wafers using lithography-free Si/SiOx patterns has already proved that high quality samples with desired geometrical parameters can be produced [22]. Moreover, we recently reported experimental results on circular dichroism in the same kind of structures [11,23]: in reference [23] we applied the photo acoustic spectroscopy to measure the resonant absorption peaks due to the excitation of weakly-guided modes, while in [11] we reported on circular dichroism when these NW are hybridized with Au.

Here we numerically investigate the same structures in the near field regime by evidencing that the NW geometry allows for the coupling of the visible light to the weakly guided modes that propagate along the NW, and are evanescent perpendicularly; a similar concept has predicted the formation of transverse spin in [24]. Then we numerically show that the evanescent part of the resonant modes generates regions of enhanced optical chirality, and we show the spatial and intensity manipulation by investigating different excitation schemes (incident angle and polarization). We then discuss on the practical implementation by including the influence of the substrate on the C distribution. We further investigate C enhancement in NWs non-uniformly covered by Au that possess broken symmetry. The role of the gold layer is both of enhancing the value of C and to create a region that can be functionalized in order to bind molecules for further fluorescence experiments.

We finally show that it is possible to control the map of the optical chirality in order to have regions of enhanced values of the same sign in the proximity of the gold-plated surfaces. Our results confirm that such structures could be used as a platform for efficient enantioselective spectroscopy.

Optics EXPRESS

2. Structure and design

The investigated structures are GaAs NWs with hexagonal cross sections sketched in Fig. 1(a), defined by their length L and radius r. As shown in [25], the optical response of ensembles of these NWs is greatly governed by the single NW behavior. We have therefore used a commercial-grade simulator based on the 3D Finite Difference Time Domain (FDTD) method in Lumerical [26] to simulate the absorption cross-section of the single NW. The vertical NW was surrounded by a simulation region limited by perfectly matched layers (PML) in all directions; PMLs were place at least half the maximum wavelength far from the NW surfaces to ensure the convergence of the calculations. Optical properties of the materials were taken from the Lumerical database (e.g. GaAs from Palik, Au from Johnson&Christy) and fitted in the excitation wavelength range. The computational mesh around the NW was 1nm in *x* and *y* directions, and 20nm in *z* direction. NW was excited by a total-field scattered source (TFSF) and the absorption cross section spectra was calculated by surrounding the NW with a box in the total field region. To simulate the electrical and magnetic field confinement, the cross-sectional field profile monitors were placed in *xy* planes. In Fig. 1(b) we show the absorption cross-section dependence of such NW on the core radius, when L = 2μm. For the core radiuses from 50nm to 80nm, we clearly see the resonant absorption peak corresponding to the excitation of the lowest mode HE_{11}. Such modes have been investigated numerically in [25,27,28]; the existence of real transverse wavevector components leads to the transverse leaking of these modes. Their fields are confined on the borders of NW (contrary to the guided modes), but the reflection from the end facets of long finite NW, under proper phase matching condition, can make them guided. These fields have transverse evanescent components, and we expect C to be the greatest where the confinement of the fields is highest, with the condition imposed by Eq. (1). Therefore in Fig. 1(c) we investigate the coupling strength as a function of the NW length. Here we chose r = 75nm which previously provided stronger coupling with respect to lower values. As expected, the absorption cross section increases for longer NWs; however, considering typical fabrication parameters we choose L = 6μm. In Fig. 1(d) we show the absorption section for the chosen parameters. As the hexagonal cross-section distinguishes HE_{11x} and HE_{11y} modes due to the symmetry reduction, we have investigated both cases of excitation with respect to the incidence plane: when electric field is polarized along *x*-axis, i.e. *p*-polarized, and when it is polarized in y direction, i.e. *s*-polarized. As it will be shown later, these two excitations correspond to different C distributions. The resonant wavelength for different polarizations does not differ for these geometric parameters, and in Fig. 1(e) we show electric and magnetic field magnitudes for *p* and *s* polarizations at the resonance λ = 796nm, taking the cross section at h = L/2 = 3μm.

Optics EXPRESS

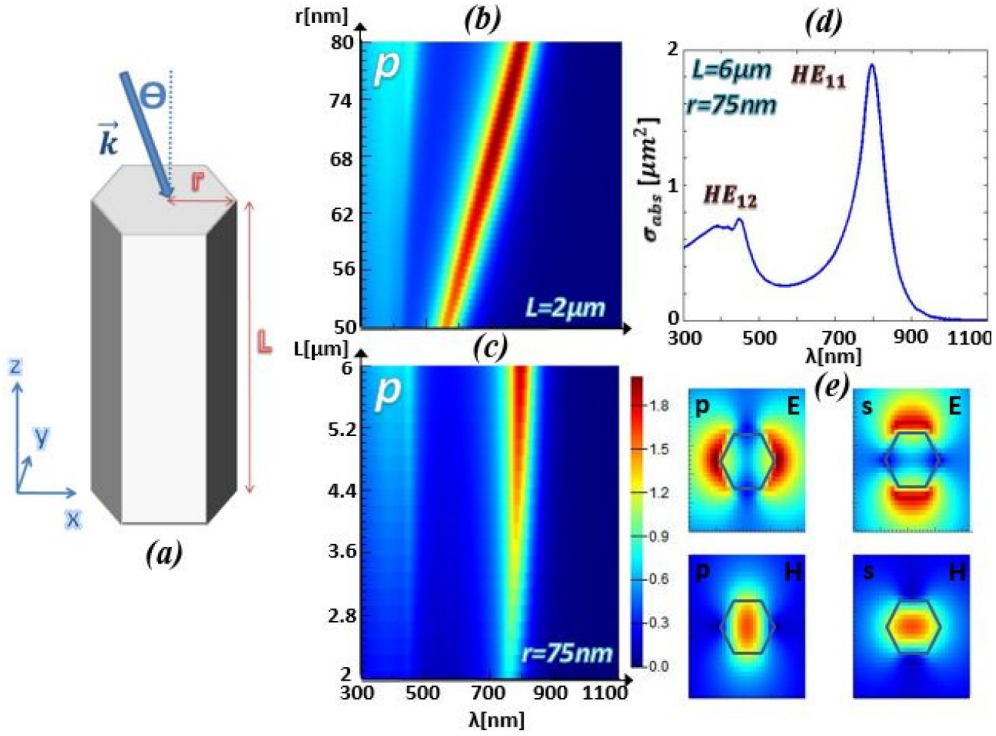

Fig. 1. (a) Schematic of NW investigated: it is defined by the radius r (equal to the side) and the length L. (b) Absorption cross section of the single NW: dependence of 2μm long NW on the radius. (c) Absorption cross section of the single NW: dependence on the length for r = 75nm. (d) Absorption cross section for L = 6μm and r = 75nm. (e) Electric and magnetic field distributions for the resonance at λ = 796nm for *p* and *s* polarizations.

3. Results and discussions

In the following we investigate the conditions for the formation of chiral fields around GaAs-based NW. We collected the electric and magnetic fields from a 3D field-profile monitor surrounding the NW. In Figs. 2(a) and 2(b) the vector plots of electric and magnetic fields are shown for s-polarization at the resonance. The electric field shows maxima in the direction of the incident polarization, as well as the non-trivial ellipticity, as shown in [24]. Magnetic field shows maxima in *xz* plane, and these two vectors are seemingly parallel at some positions where they overlap – this indicates that C can be formed in the near field, if these vectors are out of phase. Indeed, in Fig. 2(c) we plot C distribution when *s*-polarized light is resonant with NW. C is normalized to the case when the same simulation is done for the circular field of the same wavelength propagating in free space. We clearly see symmetric sign-switching non-zero lobes. If we change the polarization to *p*, C distribution changes due to the different localization of electric field maxima and their overlap with magnetic field, and the lobes switch the sign, Fig. 2(d). We can conclude that near fields around hexagonal NW have nonzero chirality in an achiral structure when it is excited by linear polarization. Due to the overall symmetry of the nanostructure, this chiral fields would vanish when integrated over the whole space. Moreover, in the vicinity of the structure normalized C is smaller than 1, which is not particularly efficient for the applications. Finally, the spatial tuning of this field is desirable. In the further work we first comment on incidence angle control of chiral fields. We propose a way to enhance C by adding the symmetry-breaking layer of gold. Finally, we discuss the influence of another layers and substrate, important for applications.

Optics EXPRESS

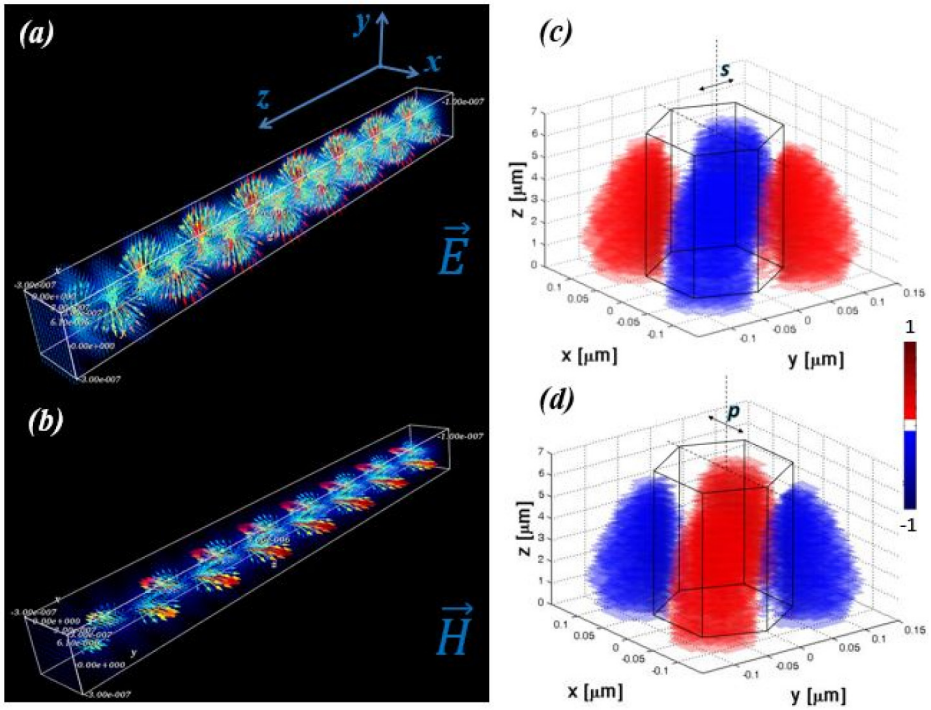

Fig. 2. (a) Electric field in the NW at the resonance. (b) Magnetic field in the NW at the resonance. (c) Chiral field distribution at the normal incidence, for *s*-polarization, normalized with respect to the value for a free space propagating circularly polarized wave. (d) Chiral field distribution at the normal incidence, for *p*-polarization, normalized with respect to the value for a free space propagating circularly polarized wave.

3.1 C distribution dependence on the incidence angle

In the following we investigate how it is possible to change the map of the near field optical chirality by varying the incidence angle and the polarization of the pump field. The plane of incidence is *xz* plane. In order to keep the single wavelength that correspond to HE_{11} excitation, we investigate smaller incident angles (greater angles would considerably shift the resonant wavelength). In Figs. 3(a) and 3(b) we show C distributions for *s*-polarized light and the angles 5° and 10°. The chiral field gradually moves to the (x,y_+) part of the 3D diagram, keeping its symmetry; this suggests that symmetry breaking could lead to the formation of the chiral field of the same sign in only one desired part of the volume. This can find applications in manipulation of the chiral molecules, if these are put in the NW surrounding. However, these fields are symmetric, as expected, so the overall response to the chiral fields would cancel out again. For *p* polarization C is spreads more in space when the incidence angle is increased, and its maximum intensity also slightly increases, Figs. 3(c) and 3(d). However, in most of the volume of interest C is still smaller than that of the circularly polarized light.

Optics EXPRESS

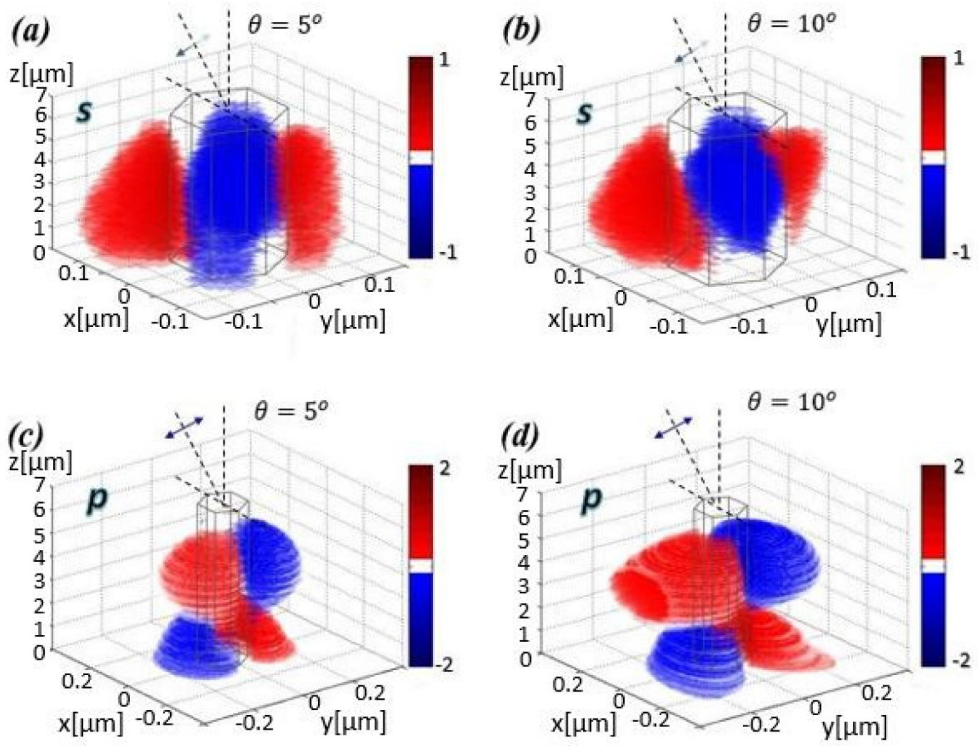

Fig. 3. (a) C distribution at the resonance for *s* polarization at 5° incidence in *xz* plane. (b) C distribution at the resonance for *s* polarization at 10° incidence in *xz* plane. The oblique incidence leads to the concentration of the chiral field in (xy_+) part of the diagram. (c) C distribution at the resonance for *p* polarization at 5° incidence in *xz* plane. (d) C distribution at the resonance for *p* polarization at 10° incidence in *xz* plane. In all cases C is normalized with respect to the value for a free space propagating circularly polarized wave.

3.2 Symmetry breaking by partial covering with gold

Here we investigate NW of the same dimensions, partially covered with Au, Fig. 4(a). We have investigated such NW in [11] where optical circular dichroism was measured by means of photo-acoustic technique. It was shown that in such NW there is still an absorption peak due to the excitation of weakly guided mode, and the experimental results were shown to be in good agreement with numerical simulations. Here we proceed with fabrication parameters taken when such NW are exposed to the flux of Au: three side-walls and Au cap is formed, and the thickness of Au layer of I (110), II (110) and the cap is 20nm, 10nm, and 20nm, respectively, Fig. 4(a). For clarity and better visualization, in the following graphs we omit the complete Au cap (we rather mark the gold-plated sides with thick yellow lines). Au layer renders this structure asymmetric in *y* direction; moreover, electric field will be differently confined for *p* and *s* polarizations, and we expect metallic layer to increase C. Au layer red-shift the resonance, so we preform simulations at 762nm and 739nm resonance, for *p* and *s* polarization, respectively. For *p* polarization we again see the symmetric pattern with four lobes, Fig. 4(b); C is more concentrated on the sidewalls without Au, but its normalized magnitude is in most of the space smaller than 1. For *s* polarization we notice that C is mainly confined in the bottom part of NW, opposite to Au sidewalls. Since there is a much larger enhancement in this case, in Fig. 4(c) we show only C>1 regions. As expected, at the normal incidence C averaged over the whole structure is still zero.

Optics EXPRESS

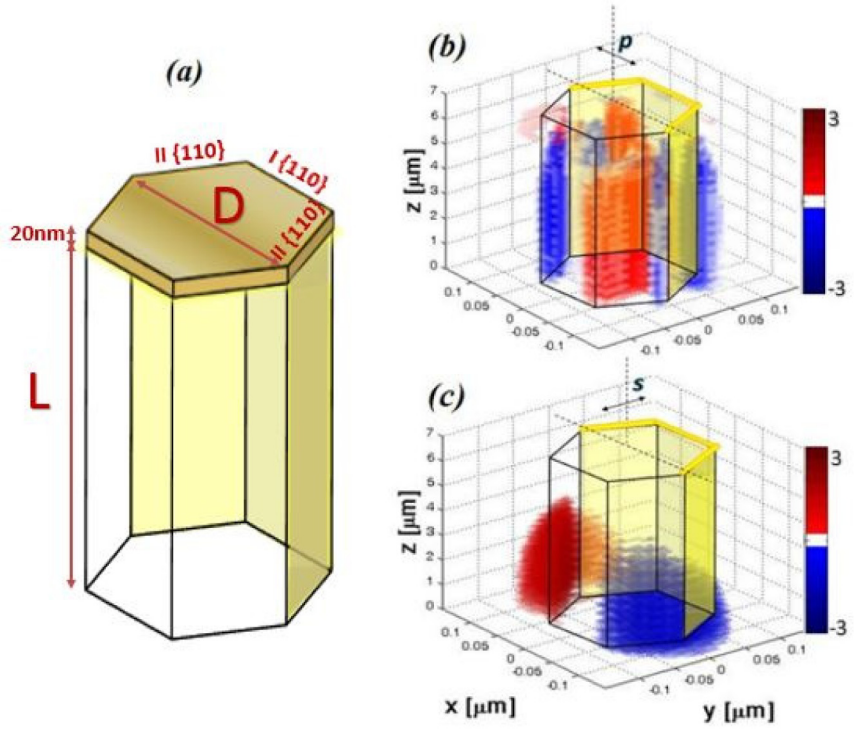

Fig. 4. (a) Schematic of NW of same L and D, partially covered with gold. The thicknesses of the sidewalls are t_I = 20nm and t_{II} = 10nm, and the cap is supposed to be uniformly 20nm thick. (b) C distribution at the resonance for *p* polarization and normal incidence. (c) C distribution at the resonance for *s* polarization and normal incidence. In all cases C is normalized with respect to the value for a free space propagating circularly polarized wave.

Next, we investigate incidence angle dependence of the *s* polarization case, Fig. 5. From the theoretical point of view explained in detail in [12] and [15], the circular dichroism due to the symmetry breaking is expected when the following vectors form a non-planar triad: the gold-plated surface normal, the NW direction and the incident wave-vector. Here the medium gold-plated surface normal is in y direction as the *x* components of the two II{110} sides cancel out, while the NW direction is always *z* direction. If the incidence plane is *xz* plane (under a non-normal incidence), these vectors indeed form a non-planar triad thus forming a system that has a different handedness when compared to its mirror image – there is no rotational or translational transformation that reproduces the original triad. Therefore, the asymmetric covering by gold renders this system chiral under a non-normal incidence in *xz* plane. On the other hand, the incident wave-vector in *yz* plane forms a planar triad with the other two vectors, which would lead to the averaged C equal to zero; this is why in further work we always consider the *xz* incidence plane. For better visualization, we show normalized C>0.8 only, and we omit the gold-plated NW sidewalls in angle dependence (they are indicated by gold colored lines on the top). With the increase of the incidence angle, positive strong chiral field is moving to the left part of the NW without Au; changing the sign of the incident angle, negative field is moving to its right part. This could be used in experiments dealing with the excitation of chiral molecules. If these are deposited onto an ensemble of these NW, one could selectively excite molecules of wanted chirality by opportunely changing the incidence angle. However, one should search for the optimization of the efficiency: the molecules that effectively react to the chirality change would be only in rather small parts of the volume with high C.

Optics EXPRESS

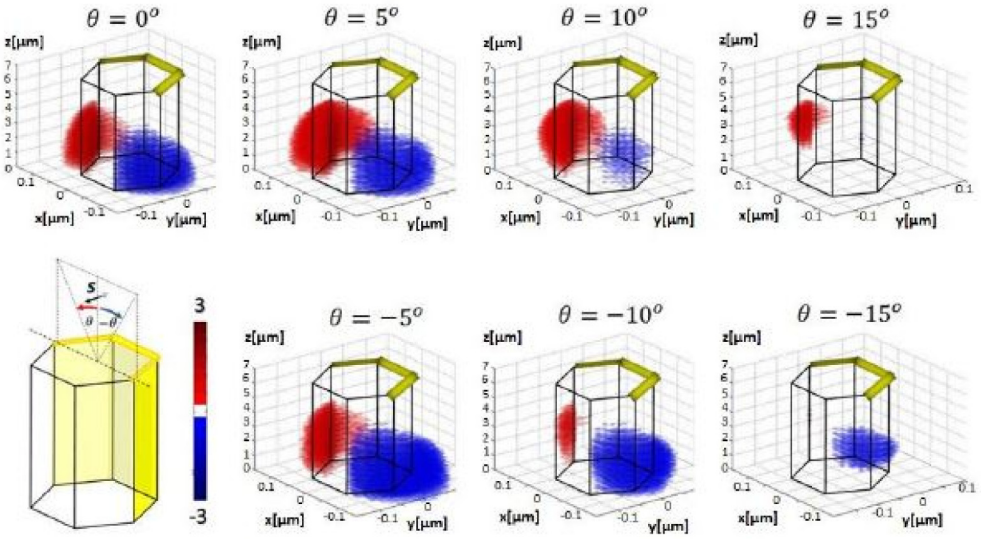

Fig. 5. C distribution dependence on the incidence angle, at the resonance with s polarization. Changing the sign of the angle changes the sign and position of the increased C distribution. In all cases C is normalized with respect to the value for a free space propagating circularly polarized wave.

3.3 Application: enantiometric spectroscopy

Finally, we propose an experiment of NW chiral fields manipulation for the indentification of chiral molecules. In what follows we have found the optimal configuration to obtain enhanced C of the same sign in the proximity of the gold-plated NW sidewalls. If we then functionalize these sidewalls with bonding molecules, they will only respond to the particular chirality sign. Instead of a free-standing single NW, we simulate C response with substrate and fabrication parameters from previous works.

GaAs-based NW are usually passivized with AlGaAs shell in order to decrease the surface recombination detrimental for optoelectronic applications. NW investigated in [11] were grown by self-catalyzed growth mode, on Si substrate. There was also a thin substrate of AlGaAs left after the shell growth, and around 70nm of Au substrate after the golden flux used to deposit golden sidewalls and the cap. We take these parameters in consideration by simulating a 6μm long NW, with GaAs core radius of 65nm and AlGaAs shell thickness of 5nm standing on Si-AlGaAs-Au substrate. We find that the resonance of such structure is at 746 nm. When increasing the angle of incidence with p-polarized light, chiral fields of the same sign are prevalently forming on the side with Au, and on the opposite side the C sign is opposite. This happens gradually starting from the symmetric case at the normal incidence, Fig. 4(b). Finally, at 20° on the golden side positive C is greatly enhanced, while negative C vanishes, Fig. 6(a); changing the angle to −20°, C inverts the sign and becomes enhanced and negative on the Au-covered sides, Fig. 6(b). For real applications we underline the advantage of the self-assembling technique from [22] to obtain the NW ensembles of uniform parameters that are fixed to the substrate and of the same orientation. In the insets of Fig. 6 we show *xy* cross-section of normalized C and the magnitude of electric field at 3μm height from the bottom. According to reference [18] for enhanced enantioselectivity we need a good overlap between C and $|E|^2$ in the regions where molecules are present; we see that the overlap between their maxima is enhanced at the left and the right corners, for 20° and −20°, respectively. We note that the values of the fields and optical chirality enhancement obtained in our structures are comparable to the results obtained by using the gammadion stars in [18] although the overlap is not as good. However, the main advantages of our geometry are given

Optics EXPRESS

by the self-assembling technique, (leading to low cost and large area samples), the possibility to control the sign of the optical chirality by varying the incidence angle (without the need to realize both left handed and right handed structures) and the large effective surface due to the extremely large surface-to-volume ratio of the vertical NWs.

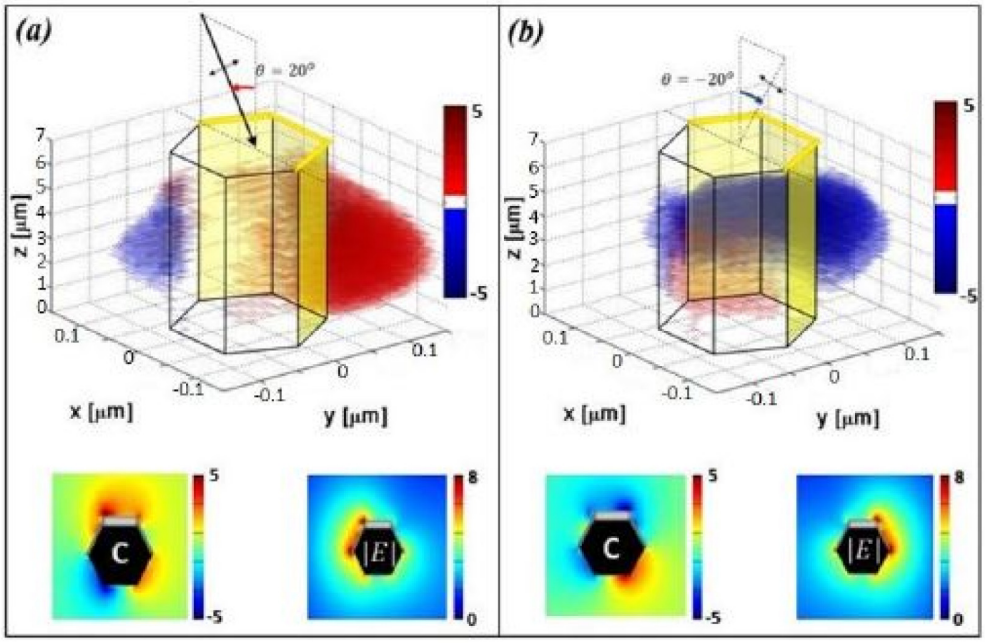

Fig. 6. C distribution dependence of GaAs-AlGaAs core-shell NW on the substrate, at the resonance. The incident light is p polarized, impinging under a) 20° incidence, and b) −20° incidence. In all cases C is normalized with respect to the value for a free space propagating circularly polarized wave. Insets are showing xy cross section of C and |E| distribution (|E| is normalized with respect the incident wave amplitude). For clarity, GaAs/AlGaAs core-shell are painted in black, while the golden part is presented in grey.

4. Summary

In conclusion, we have shown that hybrid metallo-dielectric nanostructures composed of self-assembled vertical hexagonal GaAs-based nanowires with partially Au covered sidewalls can be suitable candidates for enhanced enantioselective spectroscopy. The non-chiral geometry makes it possible to take advantage of the extrinsic chirality and to control the optical chirality in the near field by changing the angle of incidence of linearly polarized light. Enhanced chiral near-fields are created on the sidewalls of the NWs by the evanescent waves related to leaky-guided modes in the semiconductor rod. Then, the partial gold coating is responsible for: a) increased field localization by localized plasmon polariton excitation; b) symmetry breaking, leading to extended regions of high optical chirality values; c) creation of a selective reception region for biomolecules, by proper functionalization of the gold surface. The low cost realization technique combined with the field localization and the possibility to control the sign and the value of the optical chirality with linearly polarized light could be the key features for a further development of mass devices for bio-chemical sensing and pathogen detection.

Funding

Academy of Finland Project NESP (294630).